1 **The oomycete MAMP, arachidonic acid, and an *Ascophyllum nodosum*-derived plant**
2 **biostimulant induce defense metabolome remodeling in tomato**
3

4 Domonique C. Lewis[1], Timo van der Zwan[2*], Andrew Richards[2**], Holly Little[2], Gitta L. Coaker[1],
5 and Richard M. Bostock[1†]
6
7 [1]Department of Plant Pathology, University of California, Davis, CA 95616, USA
8 [2]Acadian Plant Health, Acadian Seaplants, Ltd., Dartmouth, Nova Scotia, Canada, B3B 1X8
9 [†]Corresponding author: R. M. Bostock; E-mail: rmbostock@ucdavis.edu
10
11 [*]Current address: Symvivo Corporation, Burnaby, BC, V5J 5J8, Canada
12 [**]Current address: Department of Plant Pathology, University of California, Davis, CA 95616,
13 USA
14
15
16 **Keywords:** elicitor, liquid chromatography-mass spectrometry, metabolomics, plant immunity,
17 *Solanum lycopersicum*
18
19 **Funding:** Research supported in part by a Gates Millennium Scholars Program fellowship and
20 Jastro-Shields awards to DCL, and an unrestricted gift from Acadian Seaplants, LTD., to RMB.

21 **Abstract**

22 Arachidonic acid (AA) is an oomycete-derived MAMP capable of eliciting robust defense
23 responses and inducing resistance in plants. Similarly, extract (ANE) from the brown seaweed
24 *Ascophylum nodosum*, a plant biostimulant that contains AA, can also prime plants for defense
25 against pathogen challenge. A previous parallel study comparing the transcriptomes of AA and
26 ANE root-treated tomato demonstrated significant overlap in transcriptional profiles, a shared
27 induced resistance phenotype, and changes in accumulation of various defense-related
28 phytohormones. In this work, untargeted metabolomic analysis via liquid chromatography-
29 mass spectrometry was conducted to investigate the local and systemic metabolome-wide
30 remodeling events elicited by AA- and ANE-root treatment in tomato. Our study demonstrated
31 AA and ANE's capacity to locally and systemically alter the metabolome of tomato with
32 enrichment of chemical classes and accumulation of metabolites associated with defense-
33 related secondary metabolism. AA and ANE root-treated plants showed enrichment of fatty
34 acyl-glycosides and strong modulation of hydroxycinnamic acids and derivatives. Identification
35 of specific metabolites whose accumulation was affected by AA and ANE treatment revealed
36 shared metabolic changes related to ligno-suberin biosynthesis and the synthesis of phenolic
37 compounds. This study highlights the extensive local and systemic metabolic changes in
38 tomato induced by treatment with a fatty acid MAMP and a seaweed-derived plant
39 biostimulant with implications for induced resistance and crop improvement.

40

41

42

43 **Introduction**

44 Plants have pre-formed and inducible structural and biochemical mechanisms to prevent or
45 arrest pathogen ingress and colonization. These defenses include barriers such as papillae and
46 ligno-suberized layers to fortify cell walls, and low-molecular weight inhibitory chemicals
47 (Freeman and Beattie 2008). Plants undergo transcriptional changes upon perception of
48 microbe associated molecular patterns (MAMPs) or effectors to induce local and systemic
49 resistance.

50 The oomycete MAMPs, arachidonic acid (AA) and eicosapentaenoic acid (EPA), are
51 potent elicitors of defense. These eicosapolyenoic acids were first identified as active
52 components in *Phytophthora infestans* spore and mycelial extracts capable of eliciting a
53 hypersensitive-like response, phytoalexin accumulation, lignin deposition, and protection
54 against subsequent infection in potato tuber discs (Bostock et al. 1981; Bostock et al. 1982).
55 Further work demonstrated root treatment with AA protects tomato and pepper seedlings
56 from root and crown rot caused by *Phytophthora capsici*, with associated lignification at sites of
57 attempted infection (Dye and Bostock 2021). AA has been shown to induce resistance, elicit
58 production of reactive oxygen species, and trigger programmed cell death in members of the
59 Solanaceae and other families (Araceli et al. 2007; Bostock et al. 1981; Cook et al. 2018;
60 Dedyukhina et al. 2014; Dye et al. 2020; Knight et al. 2001).

61 Phaeophyta and Rhodophyta members (red and brown macroalgae) contain numerous
62 bioactive chemicals that can elicit defense responses in plants (Klarzynski et al. 2003; Sangha et
63 al. 2010; Vera et al. 2011). The brown alga, *Ascophyllum nodosum*, is a rich source of
64 polyunsaturated fatty acids, including AA and EPA, which comprise nearly 25% of its total fatty

65 acid composition (Lorenzo et al. 2017; van Ginneken et al. 2011). *A. nodosum* and oomycetes
66 belong to the major eukaryotic lineage, the Stramenopila, and share other biochemical features
67 (e.g., both are rich in β-1,3-glucans). Commercial extracts of *A. nodosum*, used in organic and
68 conventional agriculture as plant biostimulants, may also help plants cope with biotic and
69 abiotic stresses. A proprietary *A. nodosum* extract, Acadian (hereafter ANE; APH-1011-00,
70 Acadian Seaplants, Ltd., Nova Scotia, Canada), has been shown to provide protection against
71 bacterial and fungal pathogens (Ali et al. 2016a). Studies in *A. thaliana* showed ANE induced
72 systemic resistance to *Pseudomonas syringae* pv. *tomato* and *Sclerotinia sclerotiorum*
73 (Subramanian et al. 2011). Investigation into ANE-induced resistance in *A. thaliana* and tomato
74 suggest the role of ROS production, jasmonic acid signaling, and upregulation of defense-
75 related genes and metabolites (Ali et al. 2016b; Cook et al. 2018; Jayaraj et al. 2008;
76 Subramanian et al. 2011). As a predominant polyunsaturated fatty acid in ANE, AA may
77 contribute to ANE's biological activity.

78 In a parallel study we demonstrated AA's ability to systemically induce resistance and
79 ANE's capacity to locally and systemically induce resistance in tomato to different pathogens
80 (Lewis et al. 2022). Further, we showed that AA and ANE altered the phytohormone profile of
81 tomato by modulating the accumulation of defense-related phytohormones (Lewis et al. 2022).
82 Through RNA sequencing, this same study revealed a striking level of transcriptional overlap in
83 the gene expression profiles of AA- or ANE-root-treated tomato across tested timepoints (Lewis
84 et al. 2022). Gene ontology functional analysis of transcriptomic data revealed AA and ANE
85 enriched similar categories of genes with nearly perfect overlap also observed in categories of
86 under-represented genes. Both AA and ANE treatment protected seedings from challenge with

87 pathogens with different parasitic strategies while eliciting expression of genes involved in
88 immunity and secondary metabolism. The shared induced resistance phenotype and extensive
89 transcriptional overlap of AA and ANE treatments suggested similar metabolic changes may be
90 occurring in treated plants. In the current study, untargeted metabolomic analyses were
91 conducted to assess global effects of root treatment with AA and the AA-containing complex
92 extract, ANE, on the metabolome of tomato plants.
93

94 **Materials and Methods**

95

96 **Plant growth and root treatment**

97 ***Plant materials and hydroponic growth system***

98 Seeds of tomato (*Solanum lycopersicum cv.* 'New Yorker') were surface-sterilized and
99 germinated for 10 days on germination paper. Seedlings were transferred to a hydroponic
100 growth system in 0.5X aerated Hoagland's solution contained in darkened plastic containers
101 and maintained in a growth chamber with the following conditions: light intensity 150 µmol m^{-2}
102 s^{-1}, 16-hour photoperiod, 24°C day, 22°C night, 65% relative humidity (Dye et al. 2020). The
103 seedlings are incubated in the growth chamber for approximately 10 days until emergence of
104 two true fully expanded leaves. Seed was obtained from a commercial source (Totally
105 Tomatoes, Randolph, WI).
106

107 ***Root treatment and tissue harvest***

108 Fatty acid sodium salts (Na-FA; Nu-Chek Prep, Elysian, MN) were prepared and stored as
109 previously described (Dye et al. 2020). AA stock solution was prepared by dissolving 100 mg of
110 fatty acid salt in 1 mL of 75% ethanol. AA stock solution was subsequently stored in a glass vial
111 at -20°C flushed with N_2 to minimize oxidation. A proprietary formulation of *A. nodosum* extract
112 (ANE; APH-1011-00; Acadian Seaplants, Ltd., Nova Scotia, Canada) was diluted with deionized
113 water (diH2O) to a 10% working concentration, which was used to prepare treatment dilutions.
114 All chemicals were diluted to their treatment concentrations with sterile diH_2O. Hydroponically
115 reared, 3-week-old tomato seedlings with two fully expanded true leaves were transferred to 1
116 L darkened treatment containers with their respective root treatment solutions. Following 24,
117 48, 72, and 96 hours of root treatment, tomato seedlings were removed from treatment
118 containers, and leaves and roots were excised from shoots and flash frozen in liquid nitrogen.
119 Each sample was the pool of roots or leaves of two seedlings with four replications per tissue,
120 treatment, and timepoint.
121

122 **Metabolite extraction**

123 Samples were transported on dry ice and stored at −70 °C until metabolite extraction. Tissue
124 samples were ground in liquid nitrogen using a mortar and pestle and 100 mg was weighed and
125 transferred to a 2-ml bead-beating tube containing four 2.8-mm ceramic beads. All tools and
126 consumables were pre-chilled in liquid nitrogen. After weighing, each sample was removed
127 from liquid nitrogen and kept at −20 °C until addition of extraction solution.

128 One ml of extraction solution (80 % v/v methanol and 0.1 % v/v formic acid in ultrapure
129 water) was added to each sample which was then vortexed, followed by bead-beating in a bead

130 mill (Bead Mill 24, Fisherbrand) at a speed of 2.9 m/s for one 3-min cycle. After bead-beating,
131 samples were centrifuged at 12k × *g* for 10 min at 4 °C (Accu Spin Micro 17R, Thermo Scientific).
132 Samples were diluted 5-fold using extraction solution and filtered into LC-MS-grade HPLC vials
133 using 0.22-µm PTFE syringe filters. HPLC vials were kept at 4 °C until LC-MS analysis. A blank
134 was prepared by adding 1 ml extraction solution to a bead-beating tube containing beads that
135 was processed equivalently to the samples. In addition, a quality control sample was prepared
136 by combining 20 µl of each of the extracted samples and processed equivalently.
137

138 **Liquid chromatography-mass spectrometry (LC-MS) run conditions**

139 Samples were analyzed via high performance liquid chromatography (Agilent 1260 Infinity) and
140 electrospray ionization quadrupole time-of-flight mass spectrometry (Agilent 6530 Q-TOF)
141 controlled by MassHunter software in centroid data mode. Mobile phase A was ultrapure water
142 with 0.05 % (v/v) formic acid and mobile phase B was acetonitrile with 0.05 % (v/v) formic acid.
143 Before starting the run, the column (Poroshell 120 EC-C18; 3.0 mm internal diameter, 50 mm
144 length, 2.7 µm particle size; Agilent), equipped with a guard column (EC-C18; 3.0 mm internal
145 diameter, 5 mm length, 2.7 µm particle size; Agilent), was conditioned for 20 minutes with 95 %
146 mobile phase A and 5 % B. Column temperature was maintained at 40 °C. The sample injection
147 order was randomized, with individual samples being run consecutively in positive and negative
148 mode. The quality control sample was injected at the beginning and end of the run, as well as
149 after every 12 samples throughout the run to check signal and elution stability. Source
150 parameters were as follows: drying gas temperature of 325 °C (positive) and 350 °C (negative),
151 drying gas flow 12 l/min, nebulizer pressure 35 psi, sheath gas temp 375 °C (positive) and 400

152 °C (negative), sheath gas flow 11 l/min, capillary voltage 3500 V (positive) and 3000 V
153 (negative), nozzle voltage 0 V (positive) and 1500 V (negative), fragmentor 125 V, skimmer 65 V,
154 and octopole 750 V. Acquisition was performed over a mass range of 50 to 1700 m/z using the
155 all-ions MS/MS technique, cycling three different collision energies (0, 10, 30 eV) at an
156 acquisition rate of 3 spectra/s. Simultaneous infusion of a solution of purine and hexakis(1H,
157 1H, 3H-tetrafluoropropoxy)phosphazine using the reference nebulizer was used throughout the
158 runs for mass calibration. Samples were introduced using 2 µl injections at a flow rate of 0.5
159 ml/min. A needle wash of 1:1 acetonitrile:water was used between each injection. The mobile
160 phase gradient was: 0 min, 95 % A, 5 % B; 1 min, 95 % A, 5 % B; 10 min, 50 % A, 50 % B; 15 min,
161 0 % A, 100 % B; 17 min, 0 % A, 100 % B; 17.1 min, 95 % A, 5 % B; 19.1 min, 95 % A, 5 % B.
162
163 **Data analysis pipeline**
164
165 ***Data alignment, deconvolution, and normalization***
166 Positive and negative mode raw data files from MassHunter were analysed separately in MS-
167 DIAL (v. 4.80) before downstream analysis. Tolerances for MS1 and MS2 were set to 0.025 and
168 0.075 Da respectively (Tsugawa et al. 2015). A representative quality control sample run was
169 used as the reference file to align peaks. For peak detection, the mass slice width was set to 0.1
170 DA and the minimum peak height was set to 15,000 which was approximately 3 times the noise
171 level observed in the total ion chromatogram. A linear weighted moving average method was
172 used for peak smoothing, with a smoothing level of 3 scans and a minimum peak width of 5
173 scans. Deconvolution was performed with a sigma window value of 0.5 and an MS/MS

174 abundance cutoff of 10. The adducts permitted were [M+H]+, [M+NH_4]+, [M+Na]+, [M+K]+,
175 [M+H−H_2O]+, and [2M+H]+ in positive mode, and [M−H]−, [M−H_2O−H]−, [M+Cl]−, [M+Na−2H]−,
176 and [M+K−2H]− in negative mode.
177
178 ***Quality control, feature annotation, and merging***
179 MS-DIAL data was cleaned in MS-CleanR (*mscleanr*, v. 1.0) in RStudio (v. 1.4.1106) using the
180 following parameters: minimum blank ratio of 0.8, maximum relative standard deviation of 30,
181 minimum relative mass defect (RMD) of 50, maximum RMD of 3000, maximum mass difference
182 of 0.05 and maximum retention time difference of 0.15. MS-DIAL features were clustered by
183 applying a Pearson correlation, with a minimum correlation of 0.8 and maximum p value of
184 0.05, retaining two features per cluster according to most intense and the most connected peak
185 filters (Fraisier-Vannier et al. 2020). Selected peaks were imported into MS-FINDER (v. 3.52) for
186 annotation (Tsugawa et al. 2016). Mass tolerance for MS1 and MS2 were set to 5 and 15 ppm
187 respectively, the relative abundance cut off set at 1% and the formula finder was configured to
188 use C, H, O, N, P, and S atoms. FooDB, PlantCyc, ChEBI, NPA, NANPDB, COCONUT, KNApSAcK,
189 PubChem, and UNPD were used as local databases. During the final merge step in MS-CleanR,
190 the best annotation for each peak was based on MS-FINDER scores. The normalized annotated
191 peaks list produced by MS-CleanR was used for the final statistical analyses in R.
192
193 ***Statistical analysis***
194 All statistical analyses were completed in R (v. 4.0.5) via RStudio (v. 1.4.1106). Statistical
195 analyses were run separately for each tissue type using the same parameters.

196

197 ***Multivariate analyses***

198 A partial least squares (PLS) supervised model of the complete log-transformed and Pareto-
199 scaled dataset was done using the *ropls* package (version 1.22.0), with the three treatment
200 groups as the response variables. Ellipses were drawn around treatments using *stat_ellipse*
201 (*ggplot2*) based on a 95% confidence level. This distance type considers the correlation
202 between variables and the ellipses are created around the centroid data point.
203 Heatmaps were created using the log-transformed data within the *ComplexHeatmap* package in
204 R (v. 2.13.1), with hierarchical clustering according to the complete-linkage method and
205 Euclidean distance measure across columns and rows, displayed as dendrograms.

206

207 ***Pairwise multivariate analyses***

208 Pairwise multivariate analysis was performed across all time points between ANE and H_2O, and
209 between AA and H_2O, using an orthogonal projections to latent structures discriminant analysis
210 (OPLS-DA). OPLS-DA models were generated using the *ropls* package, with the predictive
211 components set to 1 and orthogonal components to 7. S-plots were generated following
212 sample sum normalization and Pareto scaling via calculation of p1 (covariance) and pcorr1
213 (correlation) of the OPLS-DA scores using the *muma* package (v. 1.4) source code within R.
214 Chemical class enrichment analysis was achieved using ChemRICH (version 1.0 August 2020) for
215 each two-treatment comparison at each time point within R using the source code (Barupal and
216 Fiehn 2017). A student's t-test of the signal was conducted to generate p values and effect size.

217 The effect size in each case represents the difference compared to the water control treatment
218 group.
219
220 **Results**
221 ***Local and systemic metabolomic analysis of AA- and ANE- induced plants***
222 Previous transcriptomic work revealed a high level of congruency in differentially expressed
223 genes in AA- and ANE-treated tomato seedlings compared to H_2O-treated controls (Lewis et al.
224 2022). To further this line of investigation, the metabolomic profiles of AA- and ANE-root-
225 treated plants were compared to H_2O after 24-, 48-, 72-, and 96-hours exposure to their
226 respective treatments. Locally-treated roots and distal leaves were harvested, flash frozen,
227 extracted for metabolites, and subsequently analyzed via LC-MS, which with underivatized
228 samples primarily captures the nonvolatile metabolome (Tohge and Fernie 2015) (**Fig. 1A**).
229 Partial least squares (PLS) score plots of tomato root tissue revealed distinct clustering
230 by treatment irrespective of timepoint (**Fig. 1C**). No overlap was observed in the 95%
231 confidence ellipses for any treatment group. Likewise, heatmap visualization of the $\log_{10}$ signal
232 of metabolites showed clear clustering of metabolomic profiles by treatment (**Fig. 1B**).
233 Features displayed in the heatmap were filtered from the total dataset with a p-value $< 10^{-6}$ and
234 absolute fold change > 5 in roots.
235 Less defined clustering was observed in PLS score plots of distal leaf tissue across
236 sampled timepoints (**Fig. 2B**). Ellipses representing the 95% confidence interval for both H_2O
237 and AA treatments both partially overlap with the ANE treatment group. Similarly, a heatmap
238 depicting metabolite $\log_{10}$ signal showed more diffuse clustering by treatment (**Fig. 2A**).

239 Visualized metabolites from leaves displayed in the heatmap used a p-value < 0.001 and an
240 absolute fold-change > 2. These findings are reflective of distal tissue (leaves) not directly
241 treated with either elicitor. Changes in the distal leaves were not as robust as in the directly
242 treated roots, likely due to diminution of systemic signals that effect metabolic changes
243 throughout the plant.

244 An assessment of the total annotated features across the metabolomic analysis revealed
245 shared and unique annotated features between roots and leaves (**Supplementary Fig. S1A**).
246 Roots and leaves share 44 features with leaves displaying the largest number of unique
247 metabolic features (**Supplementary Fig. S1A**). There were 330 unique identified features in
248 leaves compared to 223 features unique to root tissue (**Supplementary Fig. S1A**). A comparison
249 of differential metabolic features for AA- and ANE-treated plants compared to the H_2O control
250 revealed robust overlap for both roots and leaves (**Supplementary Fig. S1B and S1C**). AA- and
251 ANE-treated roots shared 68 differential metabolic features, with AA and ANE treatments
252 possessing 37 and 29 differential features unique to each, respectively (**Supplementary Fig.**
253 **S1B**). Less overlap was observed in leaves with 39 shared differential metabolites, with AA- and
254 ANE-root treated plants displaying 34 and 19 uniquely differential metabolites, respectively
255 (**Supplementary Fig. S1C**).

256

257 ***Chemical enrichment analysis of AA- and ANE-induced plants***

258 Chemical enrichment analyses were conducted to identify classes of metabolites whose
259 accumulation was locally or systemically altered in AA- and ANE-root-treated tomato seedlings.
260 Enrichment analyses of metabolites whose mean signal was significantly changed in AA- or

261 ANE-treated plants compared to H_2O identified numerous affected chemical classes **(Fig. 3 and**
262 **Supplementary Fig. S2)**. These changes were most robust in directly treated roots compared to
263 distal leaves. Treatment of tomato seedlings with AA showed strong modulation of
264 metabolomic features classified as triterpenoids and linoleic acid and derivatives in roots. AA-
265 treated roots also showed increases in hydroxycinnamic acids and derivatives and fatty acyl
266 glycosides of mono- and disaccharides. ANE-treated roots showed modulation in the
267 accumulation of triterpenoids, steroidal glycosides, and hydroxycinnamic acids and derivatives.
268 Similar to AA-treated plants, the roots of plants treated with ANE also showed increases in
269 metabolites classified as fatty acyl glycosides of mono- and di-saccharides.
270 Although less striking than the chemical enrichment analysis of roots, leaf tissue of root-
271 treated plants did reveal an altered metabolome **(Supplementary Fig. S2)**. These changes in
272 metabolite accumulation occurred most prominently at 96 hours, the latest tested timepoint.
273 Increases in sesquiterpenoids and steroidal saponins were seen in leaves of AA-treated plants
274 at 96 hours. A mix of accumulation and suppression of terpenoids and an increase of
275 methoxyphenols was observed in the leaves of ANE-root-treated plants.
276
277 ***Specific metabolomic features modulated by AA- and ANE- root treatments***
278 Chemical enrichment analyses broadly revealed classes of metabolites that were induced or
279 suppressed in AA- or ANE-treated plants. To examine which specific variables (metabolites)
280 provide the strongest discriminatory power between the two treatment groups, a two-group
281 comparative supervised multivariate analysis, orthogonal projections to latent structures
282 discriminant analysis (OPLS-DA), was utilized. OPLS-DA score plots show strong between-group

283 variability discrimination between AA and ANE treatment groups compared to the H_2O control
284 across all tested timepoints with the x-axis describing the inter-treatment variability, and the y-
285 axis showing the intra-treatment variability **(Supplementary Fig. S3).** S-plots derived from OPLS-
286 DA were examined for both AA and ANE treatments in pairwise comparison with H_2O control. S-
287 plots of OPLS-DA revealed that treatment with AA or ANE induced shared changes in the levels
288 of several defense-related metabolites in roots **(Fig. 4)**. Variables (metabolites) with the most
289 negative and positive correlation and covariance values are the most influential in the model.
290 These metabolites are located on either tail of the S-plot (upper-right and lower-left) and
291 contribute most greatly to the separation between treatment groups
292 Bar charts depicting mean LC-MS signals for top OPLS-DA S-plot metabolites visualized
293 across all timepoints illustrate that AA and ANE have similar effects on plant metabolic response
294 **(Fig. 5)**. Treatment of tomato roots with AA and ANE resulted in a sharp increase in metabolic
295 intermediates in ligno-suberin biosynthesis. This includes AA-induced accumulation of
296 moupinamide (syn. N-feruloyltyramine) and significant increases in coniferyl alcohol in the
297 roots of ANE-treated plants across all tested timepoints. In roots, AA and ANE treatments also
298 induced increased levels of N-(p-hydroxyphenyl)ethyl p-hydroxycinnamide and N1-trans-
299 feruloylagmatine compared to H_2O treatment, reflecting strong upregulation of the shikimate
300 pathway and phenolic compound synthesis. Reduced levels of tomatine and dehydrotomatine
301 were observed in the roots of AA- and ANE-treated plants indicating suppression of steroid
302 glycoalkaloid biosynthesis. Treated plants also showed lower levels of lyso-phosphatidyl
303 ethanolamine (0:0/18:2(9Z,12Z)) that could reflect enhanced membrane lipid turnover.
304

305 **Discussion**

306 AA and ANE can induce disease resistance locally and systemically, alter the accumulation of
307 key phytohormones, and change the transcriptional profile of tomato with a striking level of
308 overlap between the two treatments (Lewis et al. 2022). The current study examined and
309 characterized the AA- and ANE-induced metabolomes of tomato. AA and ANE locally and
310 systemically induce metabolome remodeling toward defense-associated metabolic features.

311 Early studies investigating transcriptional and metabolic changes in potato revealed
312 selective partitioning and shifting of terpenoid biosynthesis from steroidal glycoalkaloids to
313 sesquiterpenes following treatment with AA or EPA or challenged with *P. infestans* (Choi et al.
314 1992; Stermer and Bostock 1987; Tjamos and Kuc 1982). Similarly, our work here with AA- and
315 ANE-treated tomato seedlings has shown a marked decrease in the levels of two abundant
316 glycoalkaloids, tomatine and dehydrotomatine **(Fig. 5)**. Our data also show strong enrichment
317 of sesquiterpenes in leaves of AA-treated plants at 96 hours post treatment, although the
318 identity of these sesquiterpenes is unresolved **(Supplementary Fig. S2A)**. This work further
319 supports evidence for differential regulation and sub-functionalization of sterol/glycoalkaloid
320 and sesquiterpene biosynthetic pathways in solanaceous plants in different stress contexts
321 (Choi et al. 1992; Stermer and Bostock 1987).

322 AA and EPA are strong elicitors that are abundant in structural and storage lipids of
323 oomycete pathogens, but absent from higher plants. Although their initial perception by the
324 plant is likely different from that of canonical MAMPs (e.g., flg22, chitosan, lipopolysaccharide),
325 there is some convergence in downstream defenses induced by these various MAMPs. Work to
326 characterize the effect of canonical MAMP treatment on the metabolomes of various plant

327 species has implicated common metabolic changes that prime for defense. Cells and leaf tissue
328 of *A. thaliana* treated with lipopolysaccharide (LPS) showed enrichment of phenylpropanoid
329 pathway metabolites, including cinnamic acid derivatives and glycosides (Finnegan et al. 2016).
330 In the same study, SA and JA were also positively correlated with LPS treatment, as we also
331 observed in tomato following treatment with AA (Finnegan et al. 2016; Lewis et al. 2022).
332 Recent work in *A. thaliana* wild-type and receptor mutants treated with two chemotypes of LPS
333 showed increases in hydroxycinnamic acid and derivatives and enrichment of the associated
334 phenylpropanoid pathway (Offor et al. 2022). Work in tobacco similarly found treatment with
335 LPS, chitosan, and flg22 all induced accumulation of hydroxycinnamic acid and derivatives, and
336 that defense responses elicited by these MAMPs were modulated by both SA and JA (Mhlongo
337 et al. 2016). More recent work in the cells of *Sorghum bicolor* treated with LPS showed
338 enrichment of hydroxycinnamic acids and other phenylpropanoids in coordination with
339 accumulation of both SA and JA (Mareya et al. 2020). Treatment of tomato with flg22 and flgII-
340 28 also enriched hydroxycinnamic acids, and tomato treatment with cps22 revealed a
341 metabolic shift toward the phenylpropanoid pathway with hydroxycinnamic acid, conjugates
342 and derivatives as key biomarkers (Zeiss et al. 2021a, b). Similar to traditional MAMPs, AA and
343 the AA/EPA-containing complex mixture, ANE, both induce enrichment of cinnamic acid and
344 derivatives in tomato seedlings **(Fig. 3)**. This supports the hypothesis that MAMPs broadly
345 induce similar metabolic changes to enrich pools of specialized secondary metabolites that
346 contribute to plant immunity.

347 AA- and ANE-treated roots showed strong enrichment of metabolic features classified as
348 fatty acyl glycosides of mono- and disaccharides **(Fig. 3)**. Fatty acyl glycosides have been

349 studied in several plant families and are most extensively characterized in members of
350 Solanaceae (Asai and Fujimoto 2010; Asai et al. 2010; Dalsgaard et al. 2006; Moghe et al.
351 2017). Investigations into the function of fatty acyl glycosides in plants suggest they may act to
352 protect against insect herbivory through various mechanisms and provide protection against
353 fungal pathogens (Leckie et al. 2016; Luu et al. 2017; Puterka et al. 2003; Simmons et al. 2004;
354 Weinhold and Baldwin 2011). A recent study isolated and identified fatty acyl glycosides from
355 strawberry capable of inducing immune responses in *A. thaliana*, including ROS burst, callose
356 deposition, increased expression of defense-related genes, and induced resistance to bacterial
357 and fungal challenge (Grellet Bournonville et al. 2020). This same work also demonstrated that
358 the strawberry-derived fatty acyl glycosides induced resistance in soybean and, due to their
359 antimicrobial activity, also protected lemon fruits postharvest from fungal infection (Grellet
360 Bournonville et al. 2020). AA- and ANE-root treatments locally elicit accumulation of the same
361 class of defense associated metabolites that Grellet et al. illustrated to have direct antimicrobial
362 activity and protect against disease (Grellet Bournonville et al. 2020).

363 Cell wall fortification is an important plant defense often initiated upon pathogen
364 infection. Cell wall lignification is a well-studied mechanism with localized accumulation of
365 phenolic intermediates and lignin at attempted penetration sites (Nicholson and
366 Hammerschmidt 1992; Vance et al. 1980; Zeyen et al. 2002). Lignification reinforces and
367 rigidifies the cell wall to create an impervious barrier to microbial ingress (Nicholson and
368 Hammerschmidt 1992; Vance et al. 1980; Zeyen et al. 2002). In our study, AA treatment of
369 tomato roots induced accumulation of a phenylcoumaran intermediate in lignin biosynthesis,
370 while ANE treatment induced accumulation of coniferyl alcohol, an important monomer unit of

371 lignin. Interestingly, coniferyl alcohol has recently been shown to act in a signaling capacity in a
372 regulatory feedback mechanism to intricately control lignin biosynthesis, an irreversible process
373 that is energetically costly (Guan et al. 2022). The findings of our study coincide with the well-
374 characterized role of lignin and its intermediates in plant defense.

375 This work characterizes local and systemic metabolic profiles of AA- and ANE-treated
376 tomato with the oomycete-derived MAMP, AA, and the AA-containing biostimulant, ANE. AA
377 and ANE profoundly alter the tomato metabolome toward defense-associated secondary
378 metabolites with notable overlap in enriched metabolite classes compared to H_2O control.
379 Further investigation is required to elucidate the functional contribution of these metabolic
380 features in AA- and ANE induced resistance and, more broadly, plant immunity. Our study adds
381 to the understanding of MAMP-induced metabolomes with implications for further
382 development of seaweed-derived biostimulants for crop improvement.

383

384 **Author contributions**

385 Study planned by all authors. Experiments performed by DCL, metabolite analyses conducted
386 by TVDZ and AR. Paper written by DCL, TVDZ, and RMB, with editing by GLC and AR.

387

388 **Literature cited**

389 Ali, N., Farrell, A., Ramsubhag, A., and Jayaraman, J. 2016a. The effect of *Ascophyllum nodosum* extract
390 on the growth, yield and fruit quality of tomato grown under tropical conditions. J. Appl. Phycol.
391 28:1353-1362.

392 Ali, N., Ramkissoon, A., Ramsubhag, A., and Jayaraj, J. 2016b. *Ascophyllum* extract application causes
393 reduction of disease levels in field tomatoes grown in a tropical environment. Crop Protect. 83:67-
394 75.
395 Araceli, A. C., Elda, C.-M., Edmundo, L.-G., and Ernesto, G.-P. 2007. Capsidiol production in pepper fruits
396 (*Capsicum annuum L.*) induced by arachidonic acid is dependent of an oxidative burst. Physiol. Mol.
397 Plant Pathol. 70:69-76.
398 Asai, T., and Fujimoto, Y. 2010. Cyclic fatty acyl glycosides in the glandular trichome exudate of *Silene*
399 *gallica*. Phytochemistry 71:1410-1417.
400 Asai, T., Hara, N., and Fujimoto, Y. 2010. Fatty acid derivatives and dammarane triterpenes from the
401 glandular trichome exudates of *Ibicella lutea* and *Proboscidea louisiana*. Phytochemistry 71:877-894.
402 Barupal, D. K., and Fiehn, O. 2017. Chemical Similarity Enrichment Analysis (ChemRICH) as alternative to
403 biochemical pathway mapping for metabolomic datasets. Sci. Rep. 7:14567.
404 Bostock, R. M., Kuć, J. A., and Laine, R. A. 1981. Eicosapentaenoic and arachidonic acids from
405 *Phytophthora infestans* elicit fungitoxic sesquiterpenes in the potato. Science 212:67-69.
406 Bostock, R. M., Laine, R. A., and Kuć, J. A. 1982. Factors affecting the elicitation of sesquiterpenoid
407 phytoalexin accumulation by eicosapentaenoic and arachidonic acids in potato. Plant Physiol.
408 70:1417-1424.
409 Choi, D., Ward, B. L., and Bostock, R. M. 1992. Differential induction and suppression of potato 3-
410 hydroxy-3-methylglutaryl coenzyme A reductase genes in response to *Phytophthora infestans* and to
411 its elicitor arachidonic acid. Plant Cell 4:1333-1344.
412 Cook, J., Zhang, J., Norrie, J., Blal, B., and Cheng, Z. 2018. Seaweed extract (Stella Maris®) activates
413 innate immune responses in *Arabidopsis thaliana* and protects host against bacterial pathogens.
414 Mar. Drugs 16:221.

415 Dalsgaard, P. W., Potterat, O., Dieterle, F., Paululat, T., Kühn, T., and Hamburger, M. 2006. Noniosides E -
416 H, new trisaccharide fatty acid esters from the fruit of *Morinda citrifolia* (Noni). Planta Med.
417 72:1322-1327.
418 Dedyukhina, E. G., Kamzolova, S. V., and Vainshtein, M. B. 2014. Arachidonic acid as an elicitor of the
419 plant defense response to phytopathogens. Chem. Biol. Technol. 1:18.
420 Dye, S. M., and Bostock, R. M. 2021. Eicosapolyenoic fatty acids induce defense responses and
421 resistance to *Phytophthora capsici* in tomato and pepper. Physiol. Mol. Plant Pathol. 114:101642.
422 Dye, S. M., Yang, J., and Bostock, R. M. 2020. Eicosapolyenoic fatty acids alter oxylipin gene expression
423 and fatty acid hydroperoxide profiles in tomato and pepper roots. Physiol. Mol. Plant Pathol.
424 109:101444.
425 Finnegan, T., Steenkamp, P. A., Piater, L. A., and Dubery, I. A. 2016. The lipopolysaccharide-induced
426 metabolome signature in *Arabidopsis thaliana* reveals dynamic reprogramming of phytoalexin and
427 phytoanticipin pathways. PLoS One 11:e0163572.
428 Fraisier-Vannier, O., Chervin, J., Cabanac, G., Puech, V., Fournier, S., Durand, V., Amiel, A., André, O.,
429 Benamar, O. A., Dumas, B., Tsugawa, H., and Marti, G. 2020. MS-CleanR: A feature-filtering workflow
430 for untargeted LC–MS based metabolomics. Anal. Chem. 92:9971-9981.
431 Freeman, B., and Beattie, G. 2008. An overview of plant defenses against pathogens and herbivores.
432 Plant Health Instr. DOI: 10.1094/PHI-I-2008-0226-01
433 Grellet Bournonville, C., Filippone, M. P., Di Peto, P. d. l. Á., Trejo, M. F., Couto, A. S., Mamaní de
434 Marchese, A., Díaz Ricci, J. C., Welin, B., and Castagnaro, A. P. 2020. Strawberry fatty acyl glycosides
435 enhance disease protection, have antibiotic activity and stimulate plant growth. Sci. Rep. 10:8196.
436 Guan, M., Li, C., Shan, X., Chen, F., Wang, S., Dixon, R. A., and Zhao, Q. 2022. Dual mechanisms of
437 coniferyl alcohol in phenylpropanoid pathway regulation. Front. Plant Sci. 13:896540.

438 Jayaraj, J., Wan, A., Rahman, M., and Punja, Z. K. 2008. Seaweed extract reduces foliar fungal diseases
439 on carrot. Crop Protect. 27:1360-1366.
440 Klarzynski, O., Descamps, V., Plesse, B., Yvin, J.-C., Kloareg, B., and Fritig, B. 2003. Sulfated fucan
441 oligosaccharides elicit defense responses in tobacco and local and systemic resistance against
442 Tobacco Mosaic Virus. Mol. Plant-Microbe Interact. 16:115-122.
443 Knight, V. I., Wang, H., Lincoln, J. E., Lulai, E. C., Gilchrist, D. G., and Bostock, R. M. 2001. Hydroperoxides
444 of fatty acids induce programmed cell death in tomato protoplasts. Physiol. Mol. Plant Pathol.
445 59:277-286.
446 Leckie, B. M., D'Ambrosio, D. A., Chappell, T. M., Halitschke, R., De Jong, D. M., Kessler, A., Kennedy, G.
447 G., and Mutschler, M. A. 2016. Differential and synergistic functionality of acylsugars in suppressing
448 oviposition by insect herbivores. PLoS One 11:e0153345.
449 Lewis, D. C., Stevens, D. M., Little, H., Coaker, G. L., and Bostock, R. M. 2022. Overlapping local and
450 systemic defense induced by an oomycete fatty acid MAMP and brown seaweed extract in
451 tomato.2022.2008.2026.505481.
452 Lorenzo, J. M., Agregán, R., Munekata, P. E. S., Franco, D., Carballo, J., Şahin, S., Lacomba, R., and Barba,
453 F. J. 2017. Proximate composition and nutritional value of three macroalgae: *Ascophyllum nodosum*,
454 *Fucus vesiculosus* and *Bifurcaria bifurcata*. Mar. Drugs 15:360.
455 Luu, V. T., Weinhold, A., Ullah, C., Dressel, S., Schoettner, M., Gase, K., Gaquerel, E., Xu, S., and Baldwin,
456 I. T. 2017. O-acyl sugars protect a wild tobacco from both native fungal pathogens and a specialist
457 herbivore. Plant Physiol. 174:370-386.
458 Mareya, C. R., Tugizimana, F., Di Lorenzo, F., Silipo, A., Piater, L. A., Molinaro, A., and Dubery, I. A. 2020.
459 Adaptive defence-related changes in the metabolome of *Sorghum bicolor* cells in response to
460 lipopolysaccharides of the pathogen *Burkholderia andropogonis*. Sci. Rep. 10:7626.

461 Mhlongo, M. I., Piater, L. A., Madala, N. E., Steenkamp, P. A., and Dubery, I. A. 2016. Phenylpropanoid
462 defences in *Nicotiana tabacum* cells: overlapping metabolomes indicate common aspects to priming
463 responses induced by lipopolysaccharides, chitosan and flagellin-22. PLoS One 11:e0151350.
464 Moghe, G. D., Leong, B. J., Hurney, S. M., Daniel Jones, A., and Last, R. L. 2017. Evolutionary routes to
465 biochemical innovation revealed by integrative analysis of a plant-defense related specialized
466 metabolic pathway. ELife 6:e28468.
467 Nicholson, R. L., and Hammerschmidt, R. 1992. Phenolic compounds and their role in disease resistance.
468 Annu. Rev. Phytopathol. 30:369-389.
469 Offor, B. C., Mhlongo, M. I., Steenkamp, P. A., Dubery, I. A., and Piater, L. A. 2022. Untargeted
470 metabolomics profiling of Arabidopsis WT, *lbr-2-2* and *bak1-4* mutants following treatment with two
471 LPS chemotypes. Metabolites 12:379.
472 Puterka, G. J., Farone, W., Palmer, T., and Barrington, A. 2003. Structure-function relationships affecting
473 the insecticidal and miticidal activity of sugar esters. J. Econ. Entomol. 96:636-644.
474 Sangha, J. S., Ravichandran, S., Prithiviraj, K., Critchley, A. T., and Prithiviraj, B. 2010. Sulfated macroalgal
475 polysaccharides λ-carrageenan and ι-carrageenan differentially alter *Arabidopsis thaliana* resistance
476 to *Sclerotinia sclerotiorum* Physiol. Mol. Plant Pathol. 75:38-45.
477 Simmons, A. T., Gurr, G. M., McGrath, D., Martin, P. M., and Nicol, H. I. 2004. Entrapment of *Helicoverpa*
478 *armigera* (Hübner) (Lepidoptera: Noctuidae) on glandular trichomes of *Lycopersicon* species. Austral
479 Entomology 43:196-200.
480 Stermer, B. A., and Bostock, R. M. 1987. Involvement of 3-hydroxy-3-methylglutaryl coenzyme a
481 reductase in the regulation of sesquiterpenoid phytoalexin synthesis in potato. Plant Physiol.
482 84:404-408.
483 Subramanian, S., Sangha, J. S., Gray, B. A., Singh, R. P., Hiltz, D., Critchley, A. T., and Prithiviraj, B. 2011.
484 Extracts of the marine brown macroalga, *Ascophyllum nodosum*, induce jasmonic acid-dependent

485 systemic resistance in *Arabidopsis thaliana* against *Pseudomonas syringae pv. tomato* DC3000 and
486 *Sclerotinia sclerotiorum*. Eur. J. Plant Pathol. 131:237-248.
487 Tjamos, E. C., and Kuć, J. A. 1982. Inhibition of steroid glycoalkaloid accumulation by arachidonic and
488 eicosapentaenoic acids in potato. Science 217:542-544.
489 Tohge, T., and Fernie, A. R. 2015. Metabolomics-Inspired Insight into Developmental, Environmental and
490 Genetic Aspects of Tomato Fruit Chemical Composition and Quality. Plant Cell Physiol. 56:1681-
491 1696.
492 Tsugawa, H., Kind, T., Nakabayashi, R., Yukihira, D., Tanaka, W., Cajka, T., Saito, K., Fiehn, O., and Arita,
493 M. 2016. Hydrogen rearrangement rules: computational MS/MS fragmentation and structure
494 elucidation using MS-FINDER software. Anal. Chem. 88:7946-7958.
495 Tsugawa, H., Cajka, T., Kind, T., Ma, Y., Higgins, B., Ikeda, K., Kanazawa, M., VanderGheynst, J., Fiehn, O.,
496 and Arita, M. 2015. MS-DIAL: data-independent MS/MS deconvolution for comprehensive
497 metabolome analysis. Nat. Methods 12:523-526.
498 van Ginneken, V. J., Helsper, J. P., de Visser, W., van Keulen, H., and Brandenburg, W. A. 2011.
499 Polyunsaturated fatty acids in various macroalgal species from North Atlantic and tropical seas.
500 Lipids Health Dis. 10:104.
501 Vance, C., Kirk, T., and Sherwood, R. 1980. Lignification as a mechanism of disease resistance. Annu. Rev.
502 Phytopathol. 18:259-288.
503 Vera, J., Castro, J., Gonzalez, A., and Moenne, A. 2011. Seaweed polysaccharides and derived
504 oligosaccharides stimulate defense responses and protection against pathogens in plants. Mar.
505 Drugs 9:2514-2525.
506 Weinhold, A., and Baldwin, I. T. 2011. Trichome-derived O-acyl sugars are a first meal for caterpillars
507 that tags them for predation. Proc. Natl. Acad. Sci. USA 108:7855-7859.

508 Zeiss, D. R., Steenkamp, P. A., Piater, L. A., and Dubery, I. A. 2021a. Altered metabolomic states elicited
509 by Flg22 and FlgII-28 in *Solanum lycopersicum*: intracellular perturbations and metabolite defenses.
510 BMC Plant Biol. 21:429.
511 Zeiss, D. R., Steenkamp, P. A., Piater, L. A., and Dubery, I. A. 2021b. Metabolomic Evaluation of *Ralstonia*
512 *solanacearum* Cold Shock Protein Peptide (csp22)-Induced Responses in *Solanum lycopersicum*.
513 Front. Plant Sci. 12:803104.
514 Zeyen, R., Carver, T., and Lyngkjaer, M. 2002. Epidermal cell papillae In: Belanger R R, Bushnell WR (ed)
515 The powdery mildew: a comprehensive treatise. APS Press, MN, USA.

516

517

518

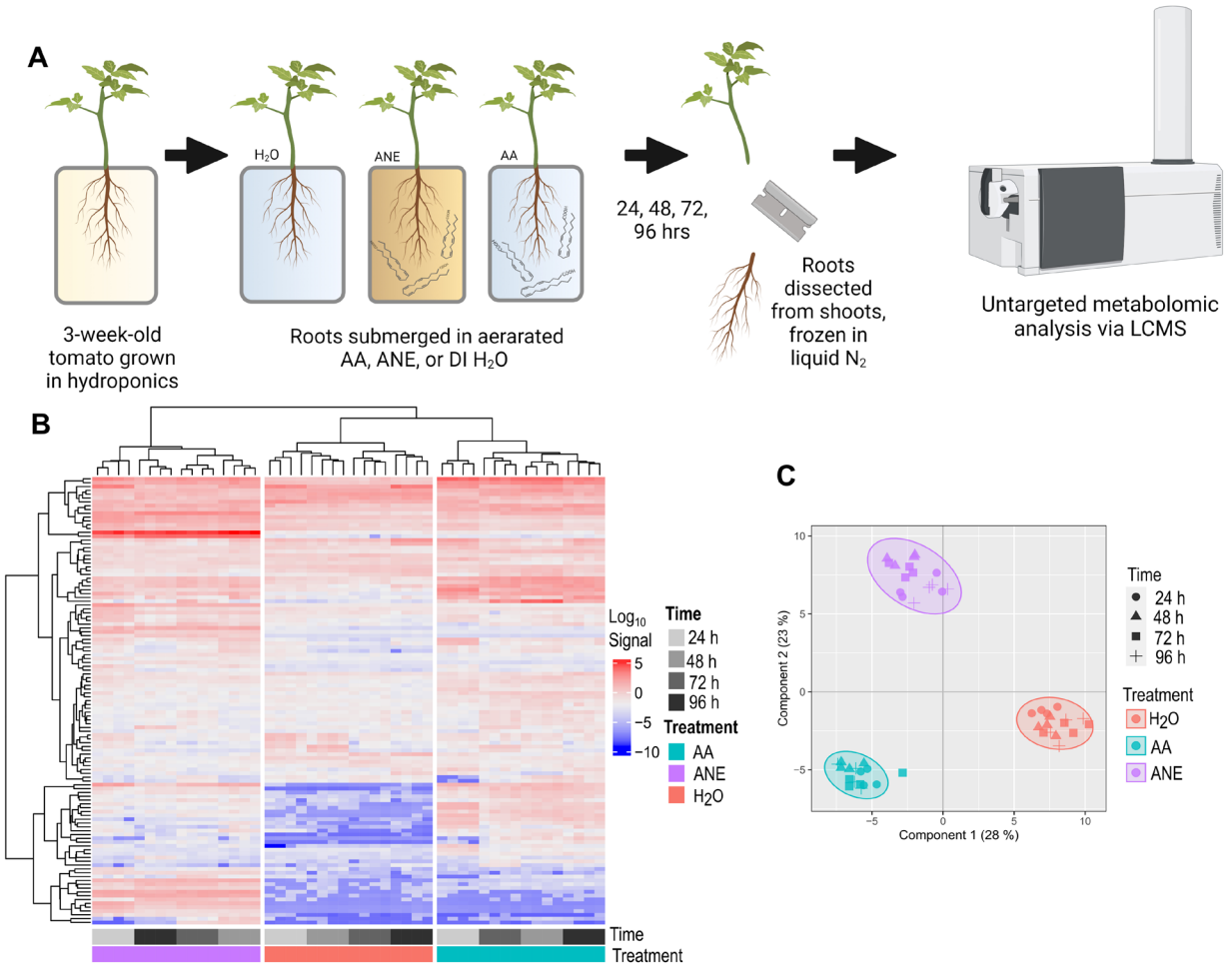

Figure 1. (A) Experimental procedure for the untargeted metabolomics study. Tomato roots were treated with 10 µM AA, 0.4% ANE, or H_2O. Following 24, 48, 72, and 96 hours of root exposure to their respective treatments, plants were harvested, root and leaf tissue dissected from shoots, and the collected tissue flash frozen in liquid nitrogen. Harvested tissue was then subjected to metabolite extraction and liquid chromatography/mass spectrometry. **(B)** Log10 signal of metabolites from root tissue of 10 µM AA-, 0.4% ANE-, or H_2O-treated plants sampled at 24, 48, 72, and 96 hours or treatment. Features visualized in the heatmap are filtered from the total dataset having an adjusted p-value < 10^{-6} and a fold change > 5. Heatmap data is log10 transformed and hierarchical clustering was conducted across rows and columns. **(C)**

529 Partial least squares score plots of tomato root metabolites after 24, 48, 72, and 96 hours of
530 treatment with 10 µM AA, 0.4% ANE, or H_2O. Ellipses indicate the 95% confidence intervals.
531 Score plots show variance of 4 biological replicates performed per timepoint and treatment.
532
533
534
535
536
537
538
539
540
541
542
543
544
545
546
547
548
549
550

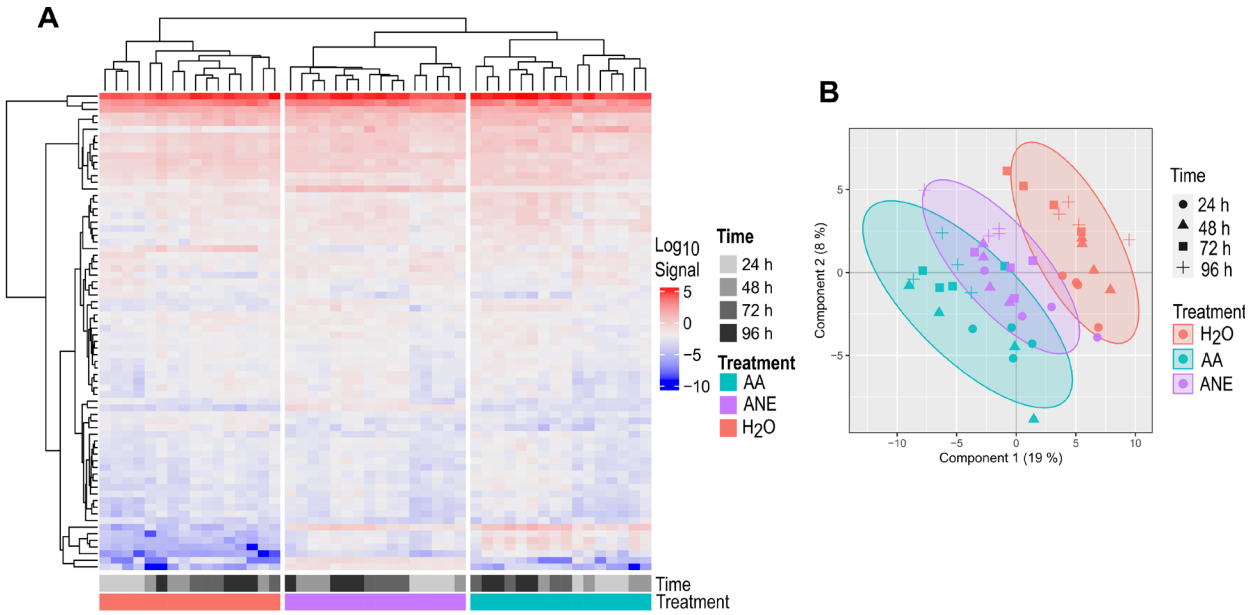

Figure 2. (A) Log10 signal of metabolites from leaf tissue of 10 µM AA-, 0.4% ANE-, or H_2O-treated plants at 24, 48, 72, and 96 hours of treatment. Features visualized in the heatmap are filtered from the total dataset having an adjusted p-value < 0.001 and a fold change > 2. Heatmap data is log10 transformed and heirachical clustering was conducted across rows and columns. **(B)** Partial least squares score plots of tomato leaf metabolites after 24,48, 72, and 96 hours of treatment with 10 µM AA, 0.4% ANE, or H_2O. Score plots show variance of 4 biological replicates performed per timepoint and treatment. Ellipses indicate the 95% confidence intervals.

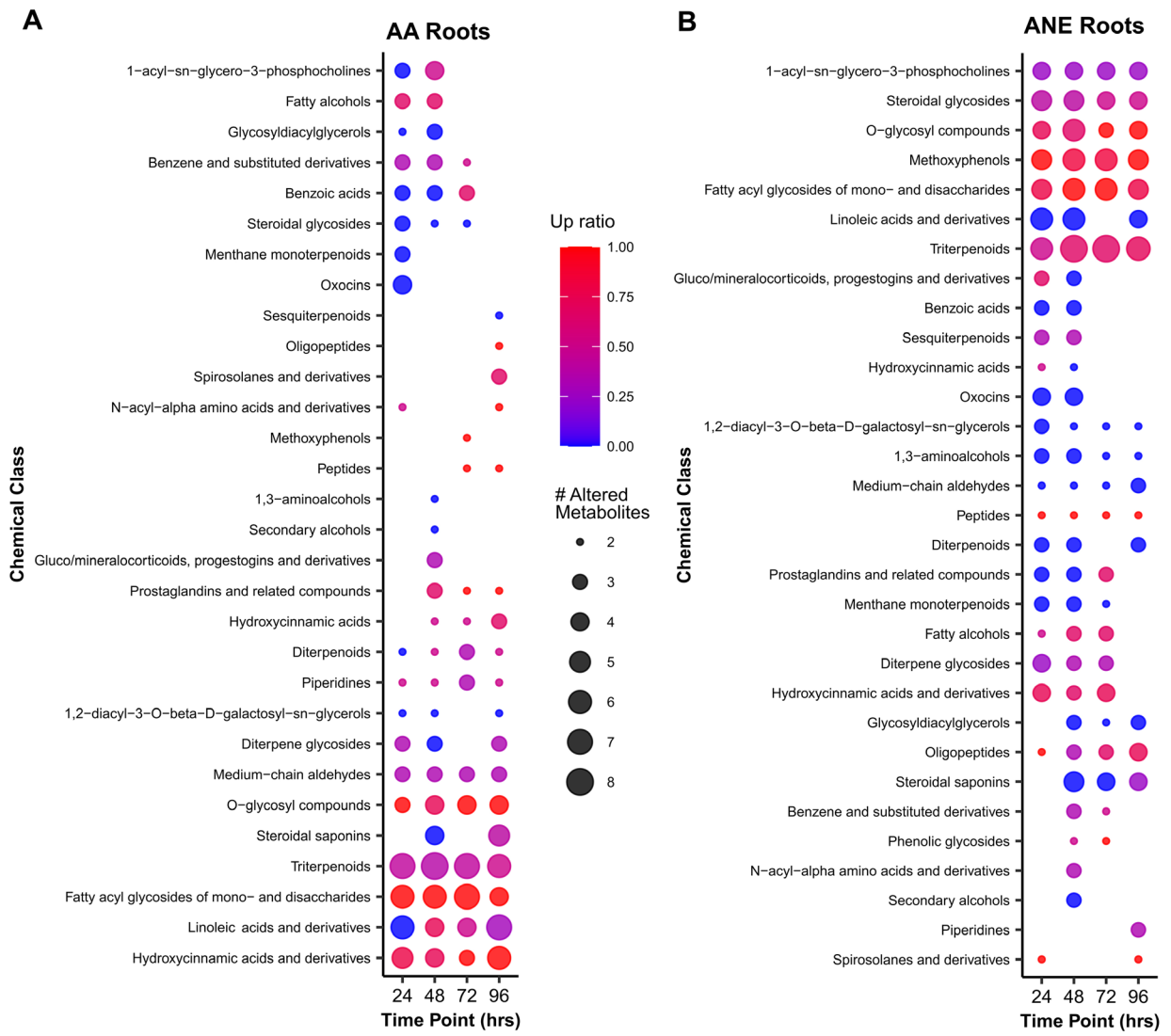

Figure 3. Dot plot illustrating chemical enrichment analysis of significantly altered metabolite clusters in roots of **(A)** AA- and **(B)** ANE-root-treated plants compared to H_2O after 24, 48, 72, 96 hours of treatment. Dot sizes indicate the number of altered metabolites per identified cluster. Dot color scale indicates the ratio of up (red) and down (blue) compounds in AA- and ANE-treated plants compared to H_2O. Up ratio represents the proportion of increased/decreased metabolites compared to H_2O.

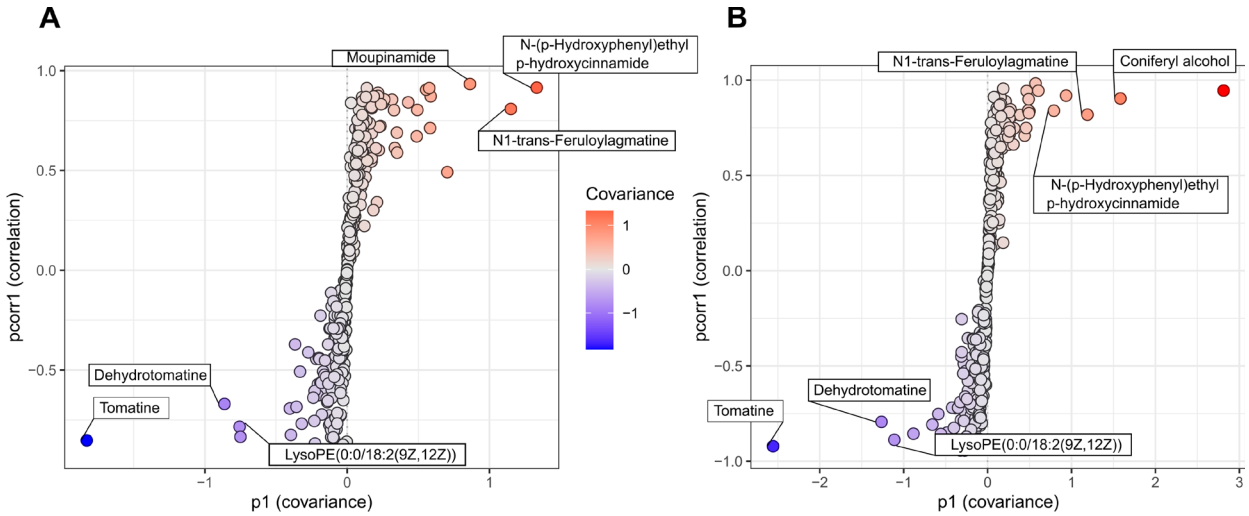

Figure 4. S-plots derived from orthogonal projections to latent structures discriminant analysis (O-PLS-DA) models for the roots of **(A)** AA-treated and **(B)** ANE-treated plants in pairwise comparison with H_2O across all tested timepoints. Color scale represents covariance strength and direction with red data points indicating most positive covariance and blue indicating most negative covariance.

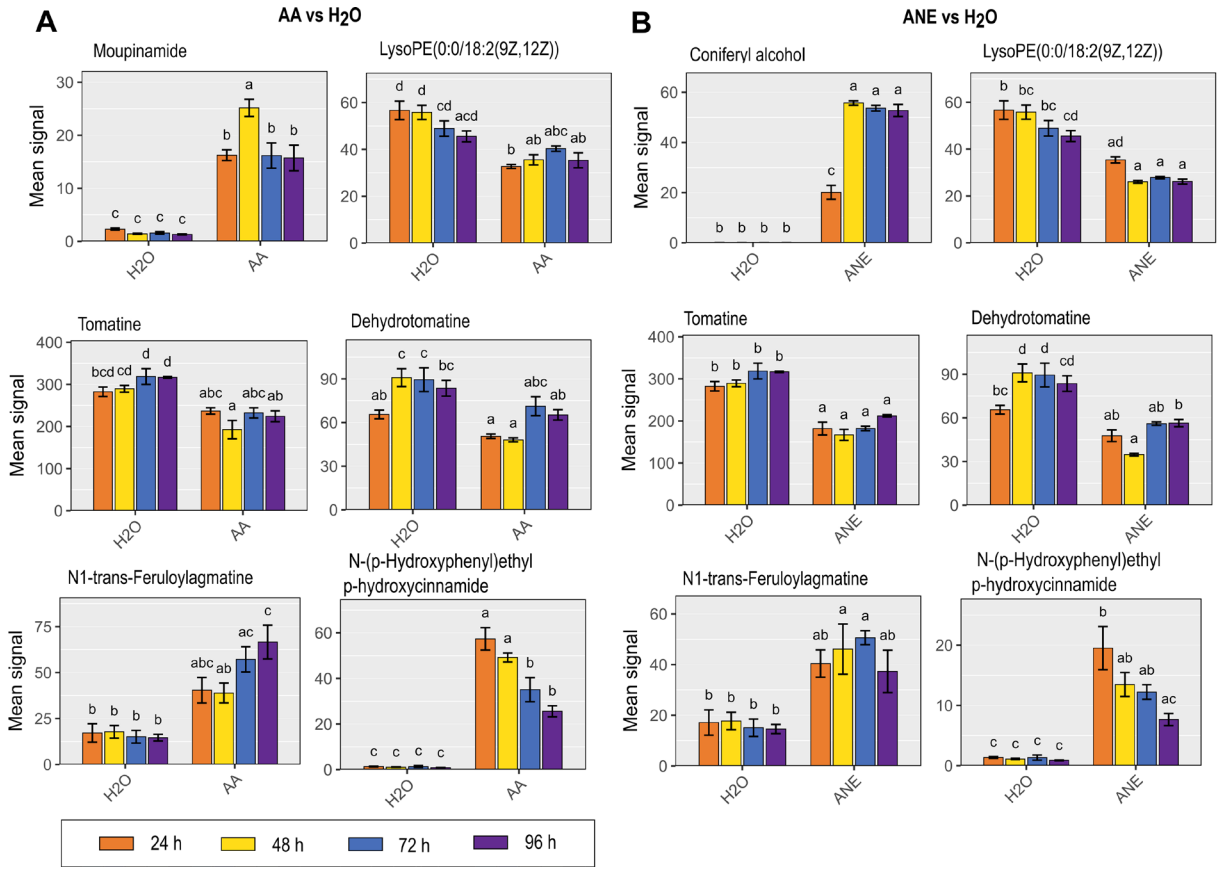

590

591 **Figure 5.** Mean LC-MS signals for the top O-PLS-DA S-plot metabolites visualized across 24, 48,

592 72, and 96 hour timepoints for **(A)** AA- and **(B)** ANE-treated roots in pairwise comparison with

593 H_2O.

594

595

596

597